KeAi

CHINESE ROOTS
GLOBAL IMPACT

Contents lists available at ScienceDirect

Petroleum Science

journal homepage: www.keaipublishing.com/en/journals/petroleum-science



Original Paper

A new type of shale gas reservoir—carbonate-rich shale: From laboratory mechanical characterization to field stimulation strategy



Zhen-Hui Bi ^{a, b}, Lei Wang ^{a, b, *}, Chun-He Yang ^{a, b}, Yin-Tong Guo ^{a, b}, Wu-Hao Guo ^{a, b}, Han-Zhi Yang ^c

- ^a Key Laboratory of Geomechanics and Geotechnical Engineering Safety, Institute of Rock and Soil Mechanics, Chinese Academy of Sciences, Wuhan, 430071, Hubei, China
- ^b University of Chinese Academy of Sciences, Beijing, 100049, China
- ^c State Key Laboratory of Coal Mine Disaster Dynamics and Control, Chongqing University, Chongqing, 400044, China

ARTICLE INFO

Article history: Received 11 April 2023 Received in revised form 19 November 2023 Accepted 22 May 2024 Available online 23 May 2024

Edited by Jie Hao and Teng Zhu

Keywords: Carbonate-rich shale Brittleness evaluation Mechanical property Lithological difference Reservoir stimulation

ABSTRACT

Recently, a new promising type of marine shale gas reservoir, carbonate-rich shale, has been discovered. But the mechanical properties of this type of shale were still unrevealed and the corresponding reservoir stimulation design was lack of guidance. Using the deep downhole cores of an exploratory carbonate-rich shale gas well, the physical and mechanical parameters and failure mechanism of the whole reservoir section were acquired and evaluated systematically, by performing XRD, tri-axial compression, Brazilian splitting, and fracture toughness tests. A new model was established to evaluate the reservoir brittleness based on fracture morphology and stress-strain curve. Recommended strategy for reservoir stimulation was discussed. Results showed that (1) Carbonate-rich shale possessed high compressive strength and high Young's modulus, which were improved by 10.74% and 3.37% compared to that of siliceous shale. It featured high tensile strength and fracture toughness, with insignificant anisotropy. (2) With the content of carbonate minerals increasing, the shear failure morphology transformed from sparse and wide brittle fractures to diffusely distributed and subtle plastic cracks. (3) The brittleness index order was: siliceous shale, clay-rich shale, carbonate-rich shale, and limestone. (4) The special properties of carbonate-rich shale were rooted in the inherent feature of carbonate minerals (high strength, high elastic modulus, and cleavage structure), resulting in greater challenge in reservoirs stimulation. The above findings would promote the understanding of carbonate-rich shale reservoirs and provide reference for the optimum design of reservoir stimulation.

© 2024 The Authors. Publishing services by Elsevier B.V. on behalf of KeAi Communications Co. Ltd. This is an open access article under the CC BY-NC-ND license (http://creativecommons.org/licenses/by-nc-nd/4.0/).

1. Introduction

Shale gas, extracted from organic-rich shale, makes up a sizeable component of the global natural gas reserves (Zou et al., 2010). Over the past decade, shale gas production has been increasing rapidly. In 2020, the global shale gas production was $768.8 \times 10^9 \text{ m}^3$ (Zou et al., 2021), with United States and China contributing $733 \times 10^9 \text{ m}^3$ and $20 \times 10^9 \text{ m}^3$, respectively (Zhang, 2021; Guo et al., 2022a). The types of shale reservoirs that have been commercially developed are marine shale, forming two national shale gas

E-mail address: lwang@whrsm.ac.cn (L. Wang).

production center (Fuling and Changning-Weiyuan) in China (Guo and Zhang, 2014; Guo et al., 2017; Xie, 2018). By comparison, marine-continental transitional shale and continental shale produce relatively little gas due to their limited reserves and weak brittleness.

In recent years, a special type of marine shale gas reservoirs, carbonate-rich shale, was encountered in the Permian stratum. Unlike previous shale types (quartz or clay dominated), the content of carbonate minerals (calcite + dolomite) became prominent, even surpassing that of quartz or clay (Liang and Li, 2021). Considering that limestone would exhibit high strength and plasticity under deep formation (Kurtulus et al., 2016; Zhang and Lv, 2020; Mo et al., 2022), the addition of such considerable proportion of carbonate minerals would make the shale present distinctive microstructure and macroscopic mechanical behavior, which further affects the

^{*} Corresponding author. State Key Laboratory of Geomechanics and Geotechnical Engineering, Institute of Rock and Soil Mechanics, Chinese Academy of Sciences, Wuhan, 430071, Hubei, China.

development strategy of this type of reservoir.

Previous geo-mechanical studies have focused mainly on the properties and mechanical characteristics of quartz-clay dominated shales (Gao et al., 2021; Wang et al., 2021b; He et al., 2022; Li et al., 2022).

In marine shales, quartz content ranged from 42 to 55.54%, carbonate minerals from 9 to 15% and clay from 25 to 37.4% (Wang et al., 2016; Chen et al., 2022; He et al., 2022; Qiu et al., 2022; Wu et al., 2022; Zhang et al., 2022). The marine-continental transitional shale exhibited 19–77.4% of clay, 21–63.27% of quartz, and 3.06–29.21% of carbonate minerals (Liang et al., 2018; Yu et al., 2019; Xue et al., 2020). While the continental shales contained 13.1–67.2% of clay and 5.8–39.3% of quartz (Tang et al., 2014; Chen et al., 2019a; Yang et al., 2019; Wang et al., 2020). To summarize, quartz is the major mineral in marine shale, while clay is the dominant mineral in marine-continental transitional shale and continental shale. Different mineral compositions will have an impact on the rock's mechanical characteristics and fracture morphology.

There is a strengthening influence of quartz content and a weakening action of clay and carbonate minerals on the compressive strength of shale (Labani and Rezaee, 2015; He et al. 2019, 2022; Hassan et al., 2019). For example, the shale with 75.30% quartz content exhibited 77.4 MPa of uniaxial compressive strength and 18.08 GPa of elastic modulus (Wang et al., 2021a); the shale with a 63.93% clay content presented 23.3 MPa of uniaxial compressive strength and 6.08 GPa of an elastic modulus (Wang et al., 2020). Studying the shale of the Niutitang Formation, Wang et al. revealed that there were two kinds of various associations between Young's modulus and quartz content (Wang et al., 2016). At quartz contents below 65%, Young's modulus increased with increasing quartz percent; at quartz contents above 65%, Young's modulus decreased with increasing quartz percent. Similarly, there were three stages (below 55%, 55%-70%, and above 70% of quartz content) in Liu's study (Liu et al., 2018). While Young's modulus correlated negatively with the amount of clay and organics (Sone and Zoback, 2013; Altowairgi et al., 2015). Moreover, the tensile strength, fracture toughness, and shear strength of shale have been studied (Shi et al., 2019; Lei et al., 2021; Lu et al., 2021; Xiong et al., 2021; Fan et al., 2022; Guo et al., 2022b; Ma et al., 2023; Wang et al., 2023). Tensile strength and fracture toughness (mode I) of the 53.41% quartz shale were 13.16 MPa and 0.96 MPa $m^{1/2}$ (Heng et al., 2020), while the value of the shale with 59.67 % clay content was 5.75 MPa and 0.30 MPa \cdot m^{1/2} (Wang et al., 2020). Shales from the Longmaxi Formation were studied by direct shear tests with cohesion and internal friction angles of 16.04 MPa and 35.34° respectively (Heng et al., 2015). In general, shale containing a high quartz content had strong mechanical properties, whereas shale possessing a high clay content showed weak mechanical features.

In quartz-rich shale, Hydraulic fractures communicating with natural fractures and beddings were used to create complex fracture networks (Tan et al., 2017; Hou et al., 2018; Song et al., 2019; Chang et al., 2022; Zhao et al., 2022). In clay-rich shale, fracture morphology would often be simple (Zhao et al. 2018a, 2018b; Wang et al., 2021b; Xu et al., 2022).

The above literature mainly discussed the properties of quartz/clay-rich shale. If the ingredient of carbonate minerals were dominated, the new type of carbonate-quartz-clay shale might show unique characteristics in mechanical properties, brittleness, and fracturing response. The physical and mechanical characteristics of this kind of shale reservoir haven't been systematically investigated, yet. Brittleness was defined as the inability to sustain plastic deformation, which affects fracturing difficulty and fracture morphology (Wang et al., 2020). Without a uniform standard, different approaches have been proposed for different purposes.

The available brittleness indices include the following: mineral composition method (Jarvie et al., 2007; Rickman et al., 2008; Jin et al., 2015; Rybacki et al. 2015, 2016), strength parameter method (Hucka and Das, 1974; Martin, 1996; Altindag, 2002; Rickman et al., 2008; Mahanta et al., 2018), strain parameter method (Hucka and Das, 1974; Martin, 1996; Hajiabdolmajid and Kaiser, 2003; Li et al., 2012), dynamic elasticity parameter method (Lai et al., 2015; Gholami et al., 2016; Rahimzadeh Kivi et al., 2017), and energy balance analysis method (Tarasov and Potvin, 2013; Ai et al., 2016; Munoz et al., 2016; Zhang et al., 2016; Rahimzadeh Kivi et al., 2018; Li et al., 2019; Wen et al., 2020). These methods were primarily focused on the stress-strain curves; however, fracture morphology was not considered, which may be also an important part in assessing of the brittleness of the rock.

In this paper, in-situ downhole full diameter cores, covering the entire reservoir formation, were collected from a typical carbonaterich shale well, with depth range of 3800~3900 m. X-ray diffraction, P-wave velocity measurements and mechanics tests (triaxial compression, Brazilian splitting and fracture toughness) were carried out systematically. The longitudinal variation of mineral composition, P-wave velocity, mechanical properties, and brittleness evaluation of the reservoir were obtained and analyzed. The distinctive physical and mechanical feature of carbonate-rich shale were revealed and comparatively analyzed with quartz/clay-rich shale and limestone. The correlation between brittleness and minerals, lithology induced mechanical difference, and the recommended strategy for reservoir stimulation were discussed.

2. Geological background

The newly discovered carbonate-rich shale gas resources were located in the Hongxing block, which ranges from Lichuan City, Hubei Province, to Shizhu County, Chongqing City, with a complete Jiannan structure that was buried at 3000-4500 m (Fig. 1a). It was estimated that 2609.8×10^8 m³ gas resources host in the area of $905~\text{km}^2$.

Based on the logs features of well logs of an exploration well HYX, the Permian system was divided into Changxing, Wujiaping and Maokou Formation. Further, Wujiaping and Maokou formation fell into two (W-1 and W-2 members) and four (M-1~4 members) members, respectively. The W-2 member contained ①—⑤ layer was the main gas-producing reservoir. Fig. 1b depicted this strata, which was obtained from an internal geological report. Sampling positions indicated by red dots, and red dotted box represented the main gas producing reservoir (W-2 member).

Influenced by the complex sedimentary environment, multiple mineral compositions and mixed lithologies were existed in the Permian system, such as limestone, siliceous shale, carbonate-rich shale, and clay-rich shale. According to the previous study, shales of the W-2 member were characterized by high brittle mineral content (63.2%), high organic matter abundance (8.87%), excellent organic matter type (II1), and well-developed organic pores (5.59%). All of these facilitate the study of regional rock mechanics for better reservoir stimulation (Wang et al., 2022).

3. Materials and test design

3.1. Sample preparation

To acquire the comprehensive mechanical features of the deep formation in the Hongxing Block, samples were taken from the HY-X exploration well. The sampling depth extended from 3833 m to 3905 m, distributed in each layer from Changxing to Maokou. Sampling details were provided in Table 1 and Fig. 2.

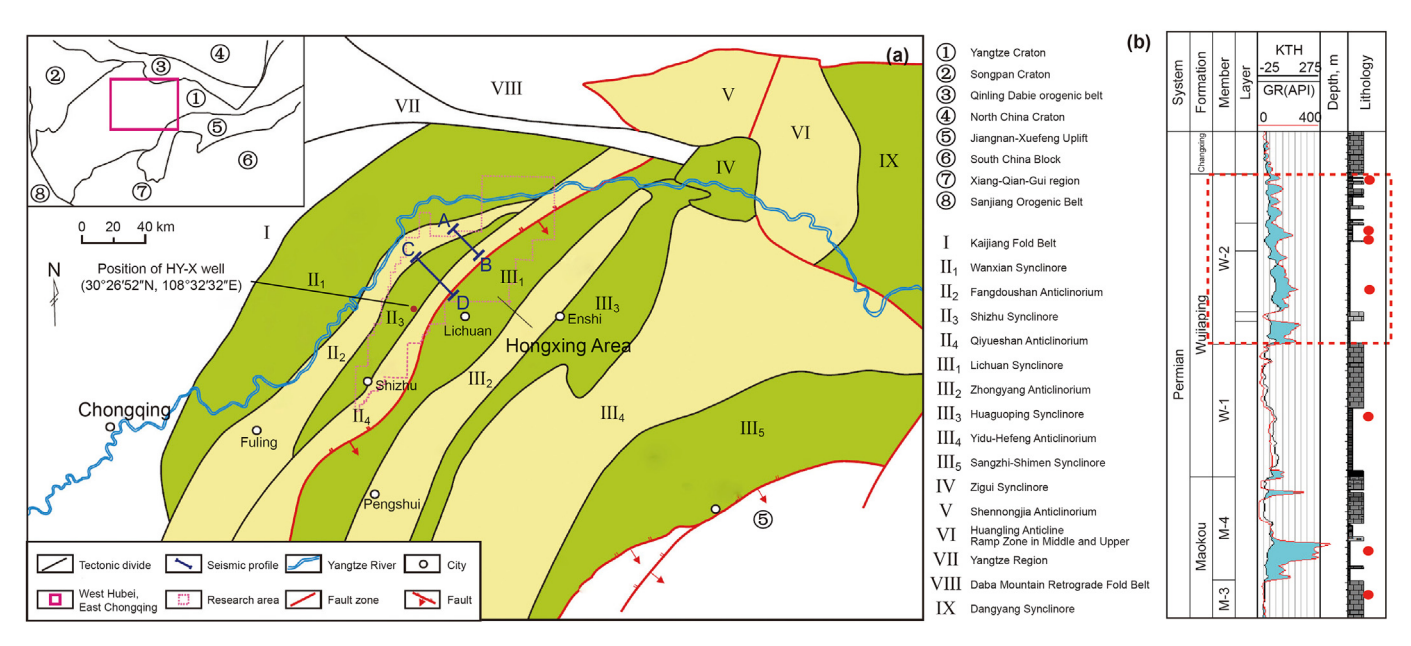


Fig. 1. HY-X well location and stratigraphic classification: (a) location map of the well, and (b) Stratigraphic delineation of the reservoir (red points represent the sampling position, and the red dotted box denoted the main production layer). Modified from (Liang and Li, 2021).

Table 1 Sampling details for HY-X well.

Formation	Member	Layer	Number	Length cm	Lithology
Changxing	_	_	GC-1	19	Limestone
Wujiaping	W-2	⑤	GC-2	15	Carbonate-rich shale
		4	GC-4	4	Siliceous shale
			GC-5	8	Carbonate-rich shale
		3	GC-7	8	Siliceous shale
		2	GC-8	9	Limestone
		1	GC-9	7	Siliceous shale
	W-1	_	GC-13	8	Clay-rich shale
Maokou	M-4	_	GC-11	10	Carbonate-rich shale
	M-3	_	GC-12	10	Limestone

Full-diameter cores (Φ 100 mm) were used to drill and process the mechanical test specimens, as shown in Fig. 3a, with the drilling direction towards the bedding. A cylinder specimen (Fig. 3b) for the triaxial compression test had a diameter of 25 mm and a height of 50 mm. The size of the Brazilian splitting tests was 25 mm \times 12.5 mm (Fig. 3c). Besides, samples subjected to fracture toughness tests were 25 mm \times 12.5 mm with a length of about 7 mm prefabricated crack in the center (Fig. 3d). Specimens were processed following the method proposed by ISRM (Hatheway, 2009) and Atkinson (Atkinson et al., 1982).

3.2. Experimental design and equipment

Following the Chinese oil and gas industry standard (SY/T) 5163–2010, the mineralogical composition of each layer sample

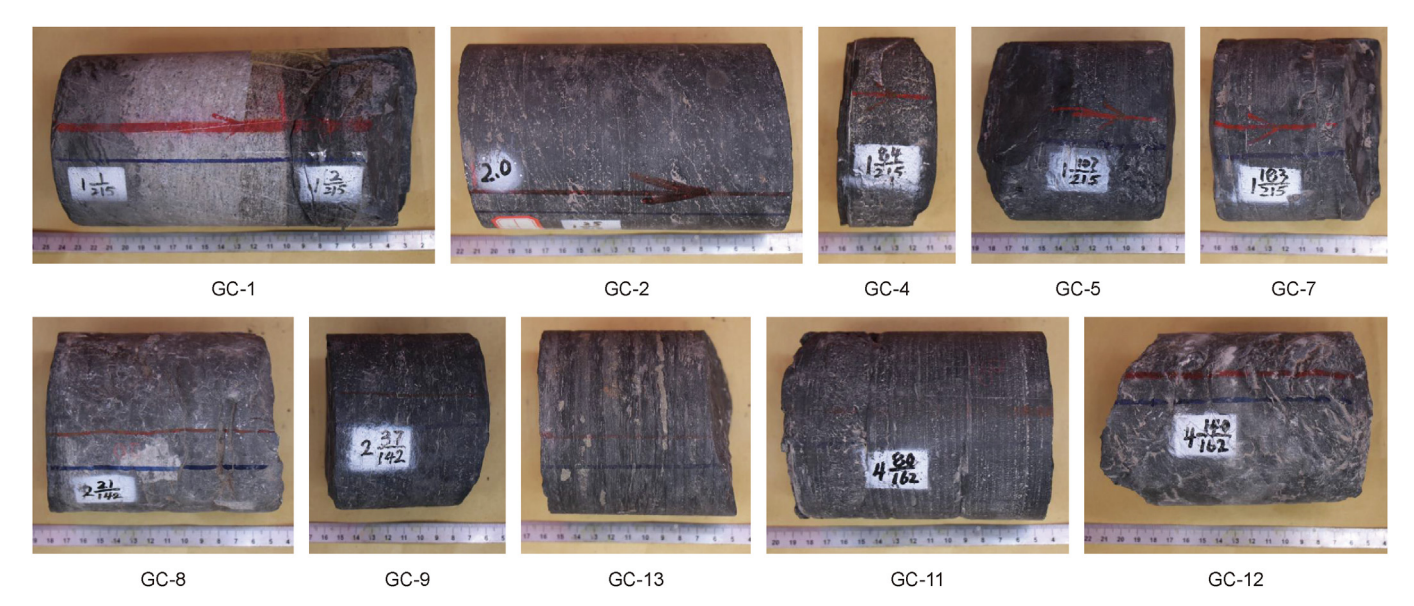


Fig. 2. Photograph of collected samples.

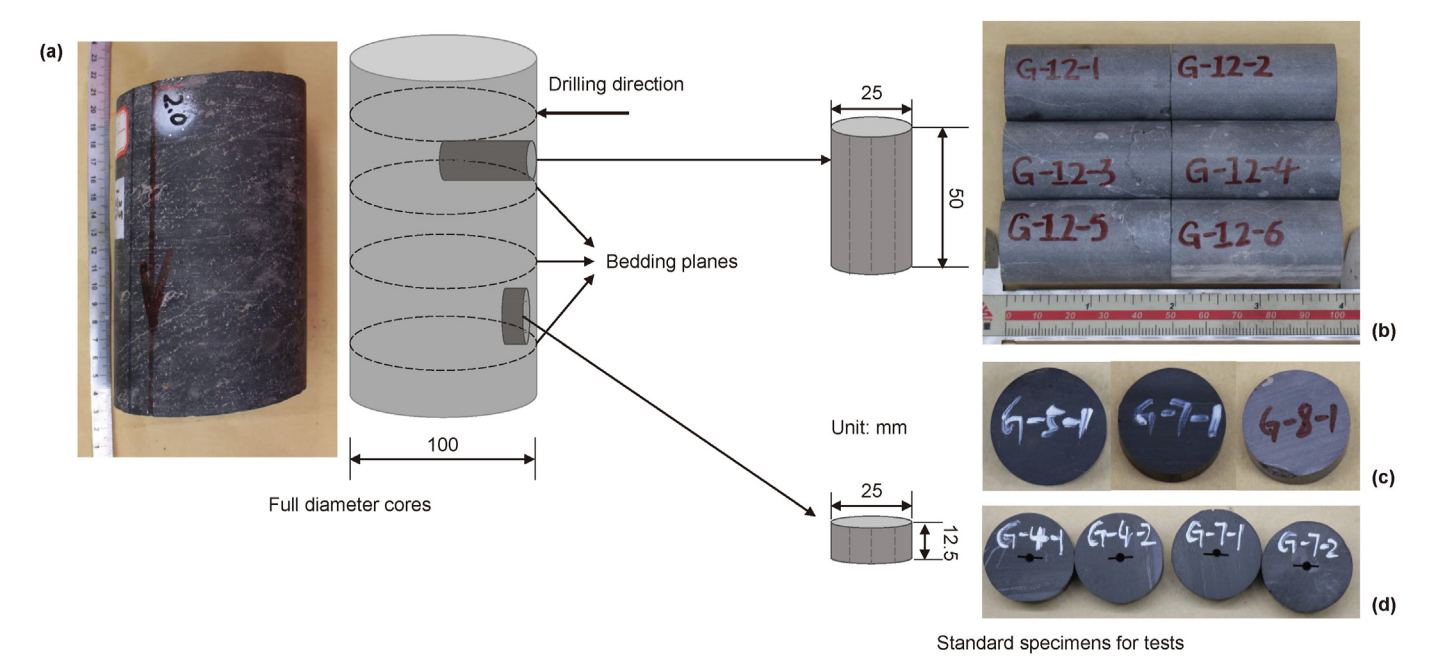


Fig. 3. Preparation of standard specimens: (a) full diameter cores, (b) tri-axial compression test, (c) Brazilian splitting test, and (d) fracture toughness test.



Fig. 4. Experimental equipment: (a) X-ray diffractometer, (b) Acoustic wave device, (c) MTS815 test system, and (d) RMT-150C test system.

was analyzed using an X-ray diffractometer (Fig. 4a). The P-wave velocity test is a widely used technique for evaluating the interior structure of rocks. To obtain the velocity, a standard specimen (Φ 25 \times 50 mm) of each layer was tested prior to the triaxial test. The test equipment is shown in Fig. 4b.

Tri-axial compression tests were performed for the samples of each layer according to the standards recommended by Hatheway (2009). To simulate the high in situ stress state, given the relatively deep burial depth of 3800—3900 m, the confining pressure was chosen to be 80 MPa. The tests were carried out on the MTS815 test system (Fig. 4c) at the Institute of Rock and Soil Mechanics, Chinese Academy of Sciences. In order to ensure that complete deformation and failure characteristics were captured, an axial displacement rate of 0.06 mm/min was adopted.

The RMT-150C test system was chosen for the Brazilian splitting and fracture toughness tests (Fig. 4d). Axial compression force was applied at a rate of 0.03 mm/min during the test. Considering the effect of the bedding plane, two loading modes were devised, where the loading force direction was either parallel or perpendicular to the plane (Fig. 5a).

During fracture toughness testing, specimens were axially compressed at an axial displacement rate (0.03 mm/min). As shown in Fig. 5b, the precast crack with the same loading direction was either perpendicular or parallel to the bedding plane. Tensile

fracture toughness (type-I) is calculated from the results of Atkinson (Atkinson et al., 1982) as follows:

$$K_{\rm Ic} = \frac{P\sqrt{a}}{RB\sqrt{\pi}} N_{\rm I} \tag{1}$$

$$N_{\rm I} = 1 - 4 \sin^2 \theta + 4 \sin^2 \theta \left(1 - 4 \cos^2 \theta\right) \left(\frac{a}{R}\right)^2$$
 (2)

where P is the maximum force on specimen, N; a is the half-length of the prepared crack, m; R is radius of specimen, mm; B is the height of specimen, mm; θ is the angle formed by the prepared crack and the loading direction, which in this case was 0. Due to difficulties in sample preparation, results were obtained for all samples except for sample GC-4, which missed the result of the Brazilian splitting test with loading direction parallel to the bedding.

4. Experimental results and analysis

4.1. Mineral compositions analysis

4.1.1. Mineral compositions

Based on XRD test, minerals, such as quartz, calcite, dolomite,

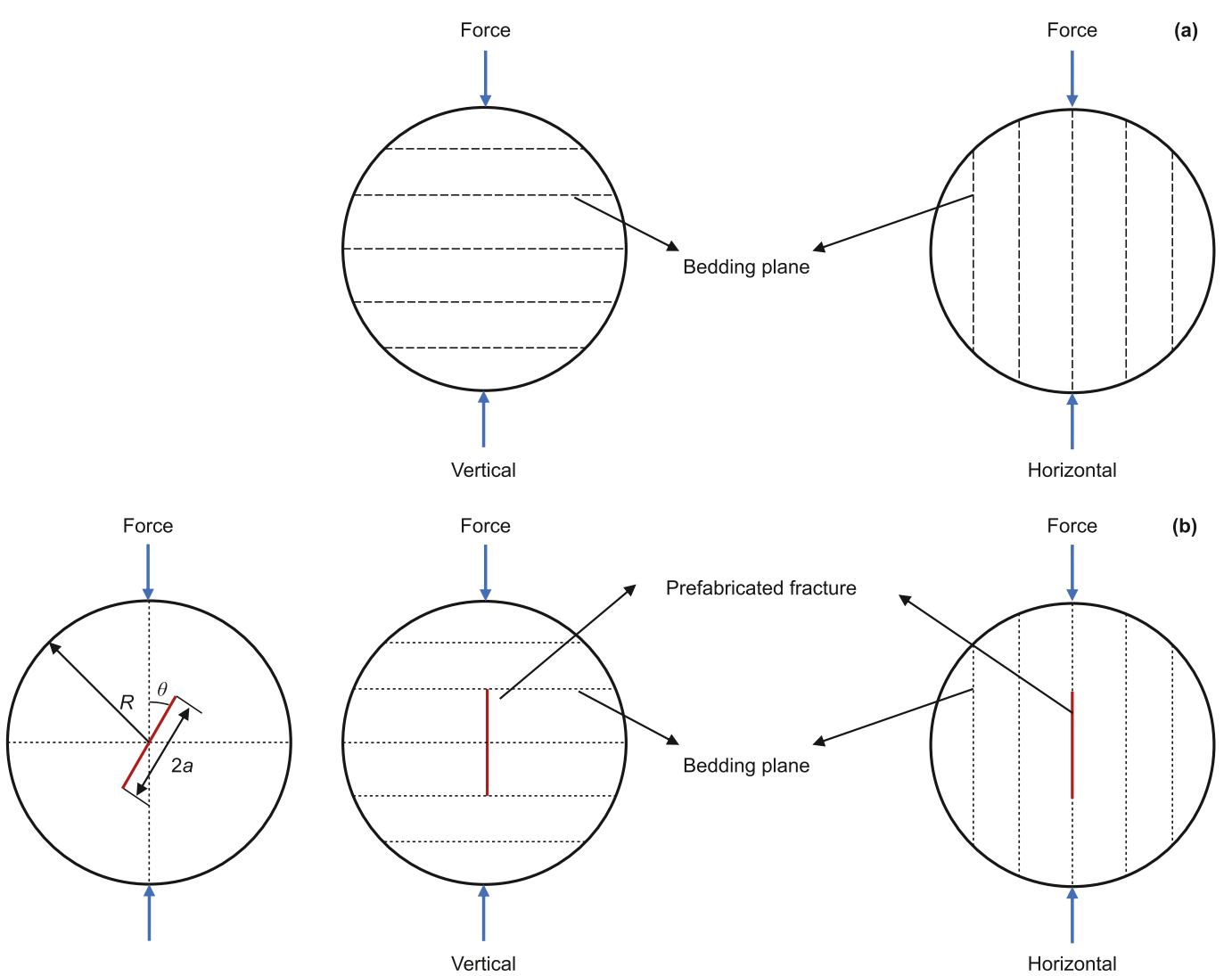


Fig. 5. Schematic of loading considering bedding effect: (a) Brazilian splitting test, and (b) fracture toughness test.

and clay, were identified, and the levels of these minerals varied greatly between layers (Appendix Table A1 and Fig. A1). With quartz, carbonate, and clay minerals as the three major compositions, all samples were classified into four lithologies:

- (1) Siliceous shale: The quartz content exceeded 45%, corresponding to cores of GC-4 (W-2-④ layer), GC-7 (W-2-⑤ layer), and GC-9 (W-2-⑥ layer);
- (2) Carbonate-rich shale: With quartz content >40% and carbonate minerals including calcite, dolomite, and ankerite >30%, typical cores were GC-2 (W-2-⑤ layer), GC-5 (W-2-⑥ layer), and GC-11 (M-4 member);
- (3) Clay-rich shale: It meant that the clay minerals content was >30% with a core of GC-13 (W-1 member).
- (4) Limestone: Carbonate minerals were enriched in the cores, for example, GC-1 (Changxing formation), GC-8 (W-2-② layer), and GC-12 (M-3 member).

4.1.2. Mineral brittleness evaluation

Various minerals contributed differently to the brittleness. Following the XRD results, the mineral brittleness index was quantitatively described using the following formulation, taking into account the mineral components and their mechanical characteristics (Huo et al., 2018):

$$a_i = E_i / \nu_i \tag{3}$$

$$A_i = a_i / a_{\text{quartz}} \tag{4}$$

$$BI_{-}M = \sum_{i=1}^{n} A_{i}M_{i} \tag{5}$$

where BI_M is the mineral brittleness index; E_i and ν_i are Young's modulus and Poisson's ratio of each mineral; a_i is the brittleness index of each mineral; a_{quartz} is the brittle factor of quartz; A_i is the relative brittle factor of each mineral to quartz, and the values of quartz, potassium feldspar, plagioclase, calcite, dolomite, siderite, pyrite, ankerite and clay are 1.00, 0.17, 0.17, 0.19, 0.36, 0.32, 1.46, 0.36, 0.05; M_i is the content of each mineral. Huo et al., (2018) proposed and discussed this method in detail.

As illustrated in Fig. 6 and Appendix Table A1, the *BI_M* values ranged from 0.196 to 0.724 for all samples. From the viewpoint of lithology, the *BI_M* values of the siliceous shale (0.629–0.724) with the most quartz content were highest in the lithology part. As the quartz content decrease, the *BI_M* values of carbonate-rich shale (0.55–0.613) and clay-rich shale (0.447) and limestone (0.196–0.415) gradually declined. Notably, the quartz content in the limestone GC-8 was relatively high, which led to its higher brittleness value.

4.2. P-wave velocity

The P-wave velocity of each sample was given in Fig. 7. The P-wave velocity were concentrated between 4500 m/s and 5200 m/s for all samples except for the sample of theW-1 member. GC-5 (W-2-④ layer) showed the maximum value of 5124 m/s, while GC-13 (W-1 member) displayed the minimum value of 3941 m/s. Ranking from the lithological perspective: carbonate-rich shale (4816−5124 m/s), siliceous shale (4603−5065 m/s), limestone (4581−4770 m/s), and clay-rich shale (3941 m/s).

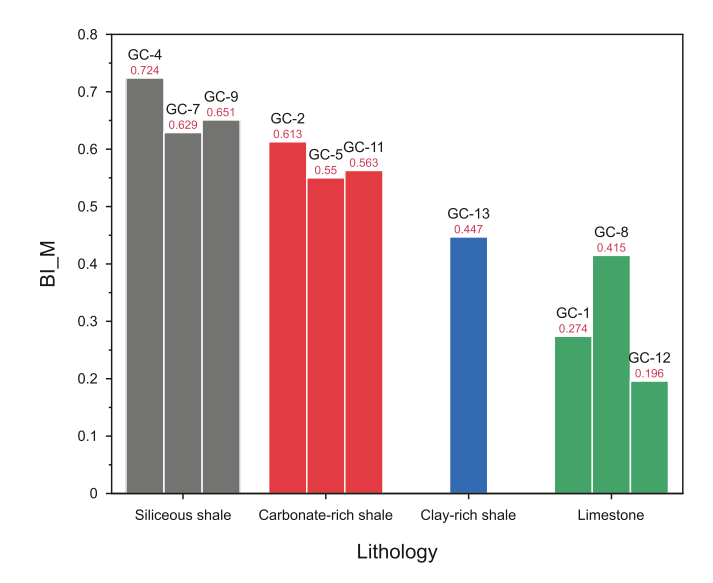


Fig. 6. BI_M of different lithologies.

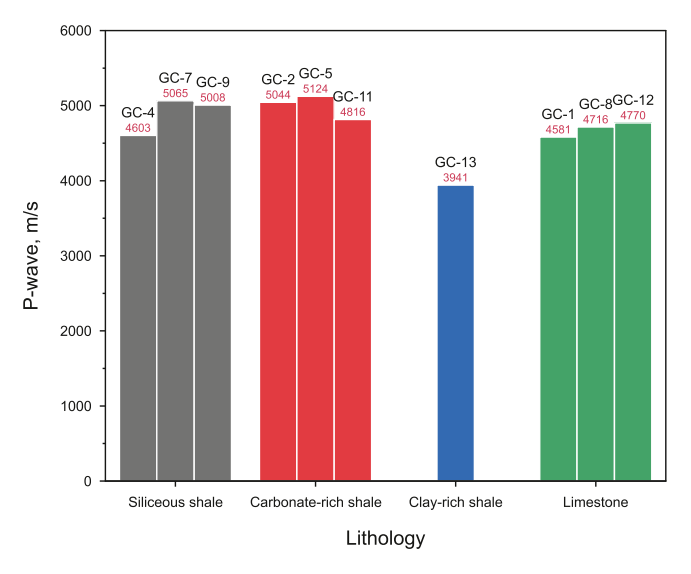


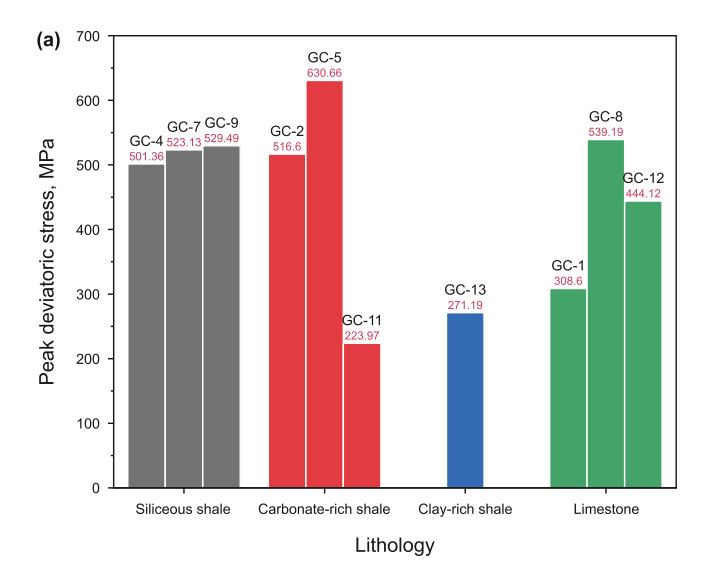
Fig. 7. P-wave velocity of different lithologies.

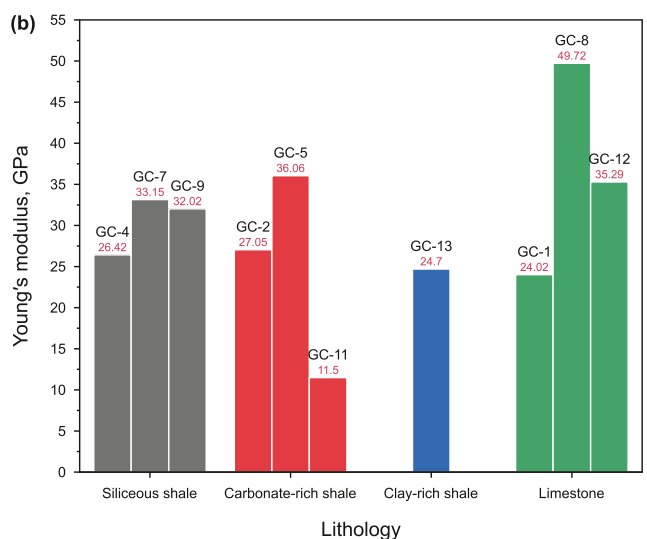
4.3. Triaxial compression tests

4.3.1. Basic mechanical parameters

The three basic parameters that are used to evaluate the mechanical properties of a reservoir in compressive testing are the peak deviatoric stress, the Young's modulus, and the Poisson's ratio.

The difference in basic mechanical parameters between different lithologies was presented in Fig. 8. The peak deviatoric stress and Young's modulus of siliceous shale ranged from 501.36 to 529.49 MPa and 26.42–33.15 GPa, respectively, which were at a high level, but with a low Poisson's ratio of 0.137–0.201. With the accumulation of carbonate minerals, the peak deviatoric stress, Young's modulus, and Poisson's ratio of carbonate-rich shale increased to 223.97–630.66 MPa, 11.50–36.06 GPa, and 0.175–0.301, respectively. However, the increase in clay minerals also affected the mechanical behavior of the rock. Compared to the other two carbonate-rich shale samples, the GC-11 sample experienced a 91%–99% increase in clay mineral content, which resulted in a 30%–50% decrease in peak deviatoric stress and Young's





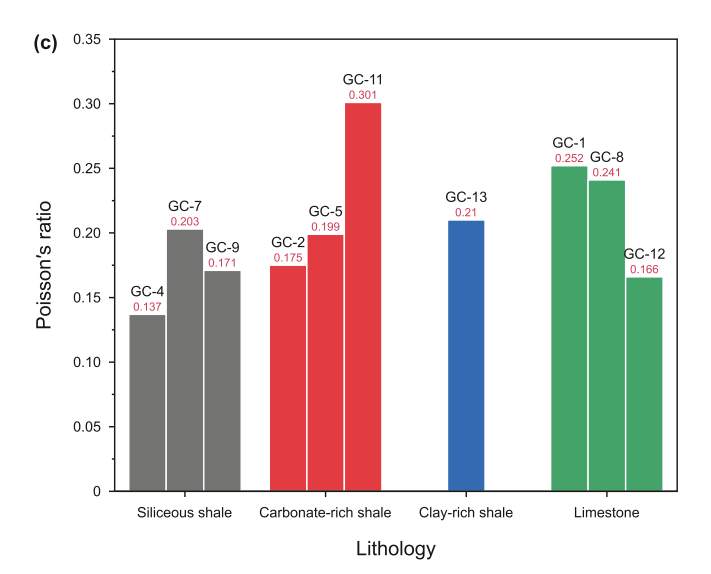


Fig. 8. Basic mechanical parameters of different lithologies: **(a)** peak deviatoric stress, **(b)** Young's modulus, and **(c)** Poisson's ratio.

modulus, and a 50%–70% increase in Poisson's ratio. Similarly, peak deviatoric stress (271.19 MPa) and Young's modulus (24.70 GPa) of clay-rich shale were at a low level, while Poisson's ratio (0.21) was high. The limestone with carbonate minerals as the main minerals exhibited lower peak deviatoric stresses (308.60–539.19 MPa), which was greater than the clay-rich shale (271.19 MPa). Young's modulus and Poisson's ratio of the limestone were at a high level, from 24.02 to 49.72 GPa and 0.166 to 0.252, respectively. The content of quartz in GC-8 samples was significant, which contributed to the high levels of peak deviatoric stress (539.19 MPa), Young's modulus (49.72 GPa), and Poisson's ratio (0.241).

4.3.2. Stress - strain curve and fracture morphology

Fig. 9 presented stress-strain curves and fracture morphologies for typical samples from different lithologies. This may provide rich and valuable information for understanding possible hydraulic fracture morphology.

In siliceous shale (Fig. 9a), the stress grew rapidly in a linear pattern to the peak without compaction and yielding stages. After reaching the peak, the stress dropped sharply, from 523.13 MPa to 241.97 MPa, with an extent of 281.16 MPa, indicating that the sample was extremely brittle. Concerning the fracture morphology, the sample exhibited shear failure, with obvious fracture width accompanied by partial bedding plane splitting, and whitish in some of the shear joints (the result of calcite mineral friction-sliding).

The sample of carbonate-rich shale exhibited a stress plateau near the peak point, showing a certain extent of plastic accumulation (Fig. 9b). The stress decreased rapidly at the post-peak stage, from 630.66 MPa to 413.26 MPa, with a decrease of 217.40 MPa, which was less brittle compared to that of the siliceous shale. For the post-test specimen, the shear cracks grew plentiful and subtle with reduced crack width, and some of the shear slip cracks were whitened and tightly closed.

As shown in Fig. 9c, clay-rich shale's stress-strain curve and fracture morphology were similar to those of brittle siliceous shale. The stress dropped from 271.19 MPa to 182.94 MPa, with a gap of 88.25 MPa. Shear cracks with large width and active bedding planes co-existed in the sample.

For the limestone (Fig. 9d), the stress experienced a marked yielding phase before the peak, followed by a slow decline to the residual stress. After destruction, the shear crack was formed but the sample was still bonded together, while more diffusely distributed tiny cracks were produced. It was a typical plastic shear failure as the specimen had an obvious bulging phenomenon.

At high confining pressure, clay minerals affected the strength of rock. There was a significant relationship between carbonate minerals and rock plasticity. As a result, when the lithology changed from siliceous or clay-rich shale to carbonate-rich shale to limestone, there was a significant transition from brittleness to plasticity in the stress-strain curves and fracture morphologies.

4.3.3. Brittleness evaluation

Brittleness evaluation is an extremely critical parameter for shale gas production. To reflect the effect of different lithology, a new brittleness index combining stress-strain curves and fracture morphology was proposed. The *BI* could be calculated as follows:

$$BI = \alpha_1 B I_1 + \alpha_2 B I_2 + \alpha_3 B I_3 + \alpha_4 B I_4 \tag{6}$$

where BI is a brittleness index comprising BI_1 , BI_2 , BI_3 , and BI_4 components; α_1 , α_2 , α_3 and α_4 are weight values of brittle composition, which are 1/4 in this paper. These values can also be assigned according to the relative importance of the different parts.

BI₁ reflected the degree of accumulation of elastic strain energy

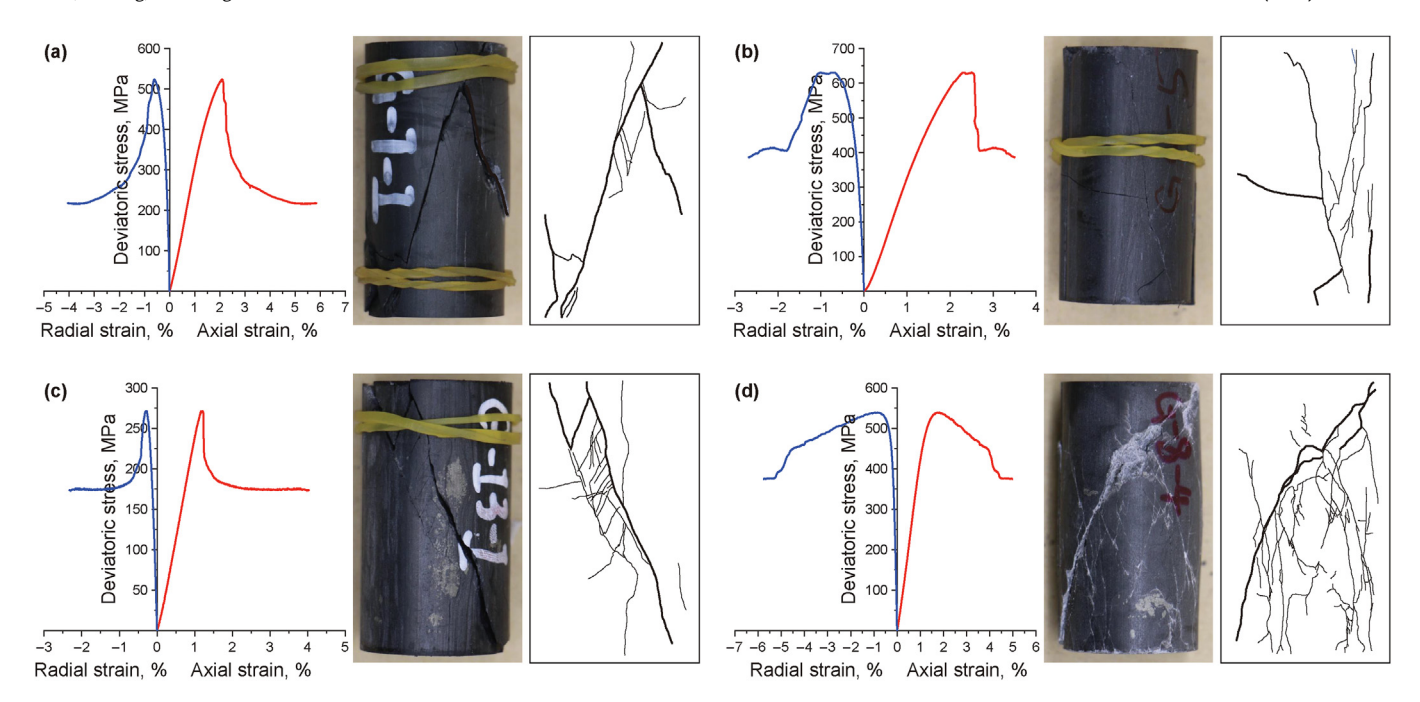


Fig. 9. Stress-strain curves and fracture morphologies of typical samples: (a) siliceous shale, (b) carbonate-rich shale, (c) clay-rich shale, and (d) limestone.

before the peak, which could be expressed as follows:

$$\begin{cases} BI_1 = \frac{U_p^e}{W_p} \\ W_p = \int (\sigma_1 - \sigma_3) d\varepsilon_1 \\ U_p^e = \frac{1}{2} \frac{\sigma_p^2}{E} \end{cases}$$
 (7)

in which U_p^e is the accumulated elastic energy; W_p is the external mechanical energy; σ_1 is the axial stress; σ_3 is the confining pressure; σ_p is the peak deviatoric stress; E is Young's modulus.

During the post peak period, Bl_2 indicated the degree of stress drop. The formula was given below:

$$BI_2 = \frac{\sigma_p - \sigma_r}{\sigma_p} \tag{8}$$

In which σ_r is the residual strength.

 BI_3 characterized the decrease rate of stress after peak. After normalization, the equation was as follows:

$$BI_3 = \exp\left[\frac{10^2(\varepsilon_p - \varepsilon_r)}{\sigma_p - \sigma_r}\right] \tag{9}$$

where ε_p is the axial strain at the peak, and ε_r is the axial strain related to the residual strength.

*BI*₄ was the part of the fracture morphology, which revealed the damage degree of each specimen. Higher values indicate higher levels of damage, i.e., greater brittleness. With normalization, the expression is shown as follows:

$$\begin{cases} BI_4 = \frac{S_i - S_{\min}}{S_{\max} - S_{\min}} \\ S_i = \frac{S_m + S_s}{S_c} \end{cases}$$
 (10)

where S_i is the density of cracked area; S_{\max} and S_{\min} are maximum and minimum densities; S_m is the area of main crack; S_S is the area of secondary cracks; S_C is the cross-sectional area (50 \times 25 mm as standard) of the sample.

The BI values were recorded in Fig. 10 and Table 2. In the vertical direction, the BI values fluctuated widely with distribution of 0.136–0.735. From the perspective of lithology, siliceous shale had the highest BI value of 0.611–0.735, followed by clay-rich shale with 0.669, then carbonate-rich shale with 0.434–0.511, and

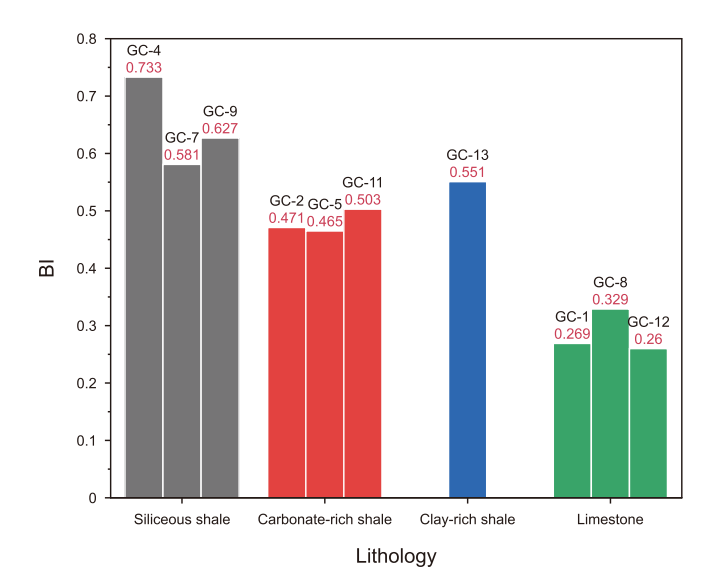


Fig. 10. BI of different lithologies.

Table 2Data collection of mechanical parameters in triaxial compression tests.

Sample	$\sigma_p(\mathrm{MPa})$	E(GPa)W	B (mJ/m 3) U_{e}	$^{B}(\text{mJ/m}^{3})$	$\sigma_r(MPa)$	$\varepsilon_p(\%)\varepsilon$	e _r (%).	$S_i(\text{mm}^2)$	$BI_1/4B$	$I_2/4$ B	$I_3/4$ E	314/4	BI
GC-1	308.60	24.02	4.99	1.98	267.79	2.36	3.81	0.006	0.0990.	033 0	.004	0 (0.136
GC-2	516.60	27.05	6.97	4.93	350.97	2.46	4.05	0.013	0.1760.	0800	.0960	.0820	0.434
GC-4	501.36	26.42	5.24	4.76	297.85	2.10	2.35	0.022	0.2270.	1010	.2210	.1850	0.735
GC-5	630.66	36.06	9.27	5.51	395.99	2.49	3.37	0.012	0.1490.	093 (0.17 0	.0650	0.479
GC-7	523.29	33.15	6.20	4.13	241.97	2.09	3.82	0.021	0.1670.	1340	.1350	.1750	0.611
GC-8	539.19	49.72	5.85	2.92	376.91	1.75	4.47	0.018	0.1250.	0750	.0470	.1340	0.381
GC-9	529.49	32.02	5.68	4.38	314.92	2.05	2.80	0.020	0.1930.	1010	.1760	.1540	0.625
GC-13	271.19	24.70	1.67	1.49	179.42	1.20	1.94	0.028	0.2230.	085 0	.112().25 (0.669
GC-11	224.12	11.50	2.89	2.18	132.77	2.27	3.28	0.018	0.1880.	1020	.083 0	.1370	0.511
GC-12	444.12	35.29	5.09	2.79	354.67	1.91	5.03	0.013	0.1370.	0500	.0080	.0760	0.271

Notes: dark, red, blue, and green represent siliceous shale, carbonate-rich shale, clay-rich shale, and limestone, respectively.

limestone with the lowest BI value of 0.136-0.381.

A variety of methods were used to calculate the brittleness. Here, three typical brittleness indices were selected for comparison from different perspectives. $BI_{(1)}$ was calculated as follows based on the mineral composition (Jarvie et al., 2007):

$$BI_{(1)} = \frac{W_{\text{qtz}}}{W_{\text{qtz}+\text{carb}+\text{cly}}} \tag{11}$$

where W_{qtz} is the weight part of quartz; $W_{\text{qtz} + \text{carb} + \text{cly}}$ is the weight part of the total of quartz, carbonate, and clay minerals.

 $BI_{(2)}$ was investigated depending on Young's modulus and Poisson's ratio, as listed below (Rickman et al., 2008):

$$BI_{(2)} = \frac{1}{2} \left(\frac{E - E_{\min}}{E_{\max} - E_{\min}} + \frac{\mu_{\max} - \mu}{\mu_{\max} - \mu_{\min}} \right)$$
 (12)

where the min and max indices were the minimum and maximum values of Young's modulus and Poisson's ratio, respectively, for the whole sample.

Considered from the point of energy conservation, $BI_{(3)}$ was shown below (Rahimzadeh Kivi et al., 2018):

$$BI_{(3)} = \frac{1}{2} \left(\frac{dW_e}{dW_r} + \frac{dW_e}{dW_{et} + dW_p} \right)$$
 (13)

where dW_e is the consumed elastic energy, dW_r is the rupture energy, dW_{et} is the total elastic energy, and dW_p is the plastic energy.

The $BI_{(1)} - BI_{(3)}$ for different lithologies were shown in Fig. 11. By comparison, it was noticed that $BI_{(1)} - BI_{(3)}$ had their limitations in evaluating the brittleness of samples with different lithologies in well HY - X. The newly proposed BI could be qualified.

4.4. Brazilian splitting test

This test investigated the influence of the loading force direction

relative to the bedding. See Fig. 12 and Appendix Table A2 for the results. Some specific tensile strengths may not be obtainable due to processing problems. When loading direction was parallel to bedding plane, tensile strength was 1.10–11.62 MPa, while when it was perpendicular, the values were slightly higher at 2.55–12.92 MPa.

Lithologically, carbonate-rich shale displayed high tensile strength values with a wide fluctuation range of 1.10–12.92 MPa. The values of limestone followed by carbonate-rich shale were 4.33–11.62 MPa. While, the values of siliceous shale and clay-rich shale were similar with 2.55–8.2 MPa and 4.83–8.5 MPa, respectively.

4.5. Fracture toughness test

During the fracture toughness test, the pre-crack directions relative to the bedding plane were considered, while the direction of loading remained the same as the direction of the pre-crack. Fig. 13 and Appendix Table A3 summarized the results. When the prefabricated crack was parallel to the bedding plane, the fracture toughness (type-I) were 0.06-0.98 MPa $\mathrm{m}^{1/2}$. In the vertical direction, the values were 0.14-0.91 MPa $\mathrm{m}^{1/2}$.

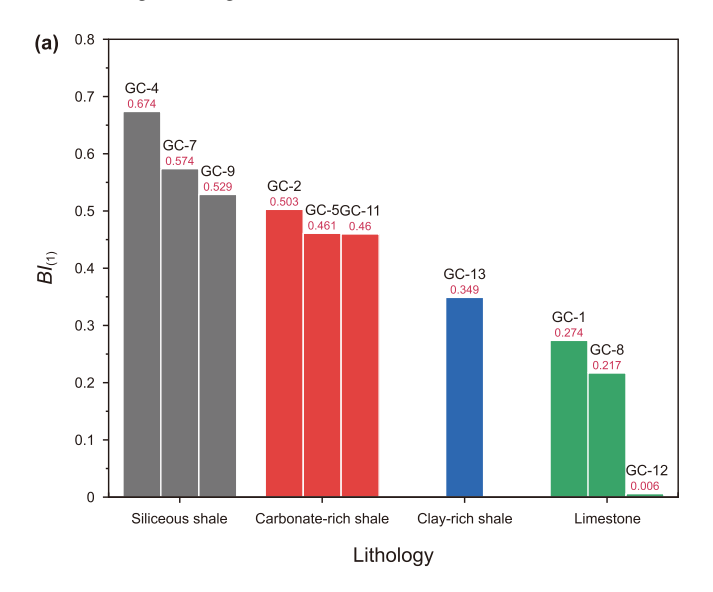
In terms of lithology, the siliceous shale was at a high level of 0.20–0.85 MPa m $^{1/2}$. The carbonate-rich shale and limestone were similar and dispersed, with 0.15–0.98 MPa m $^{1/2}$ and 0.06–0.87 MPa m $^{1/2}$, respectively. The values of clay-rich shale were 0.18–0.57 MPa m $^{1/2}$ at the lowest level.

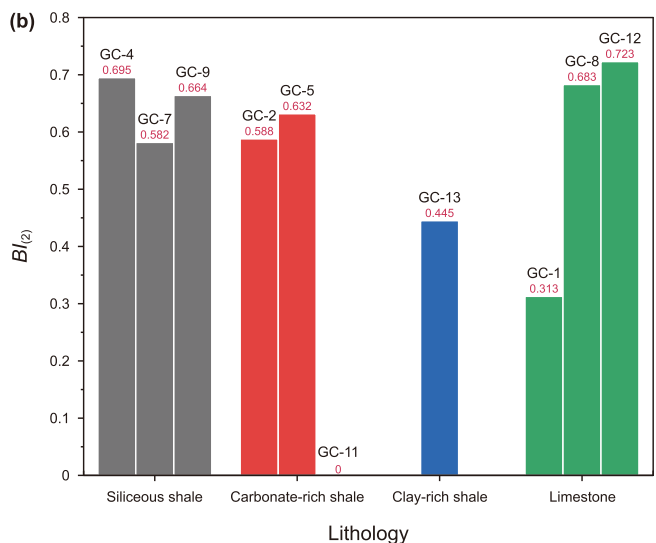
The tendency of the mineral compositions, *BI_M*, P-wave velocity, mechanical parameters, and *BI* to vary with depth was shown in Appendix Fig. A1.

5. Discussion

5.1. Correlation of BI with other parameters

Based on mineral components and stress-strain curves, BI_M and BI were relatively comprehensive brittleness indices, which





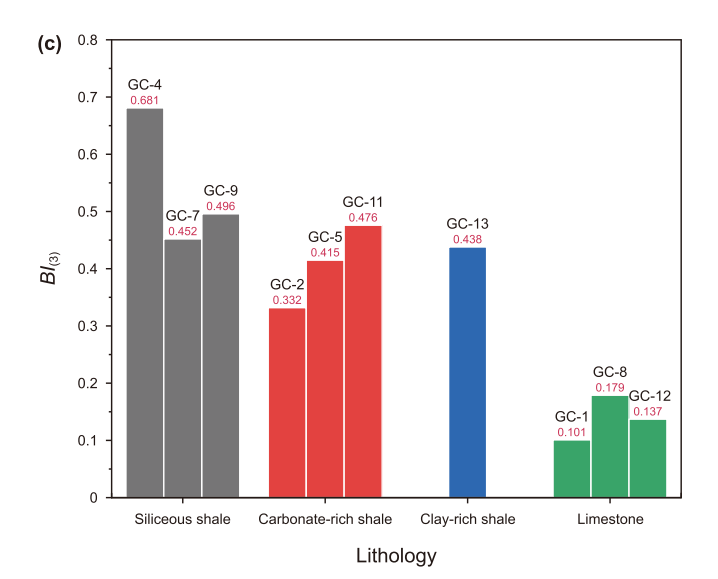


Fig. 11. BI of different lithologies: (a) $BI_{(1)}$, (b) $BI_{(2)}$, and $BI_{(3)}$.

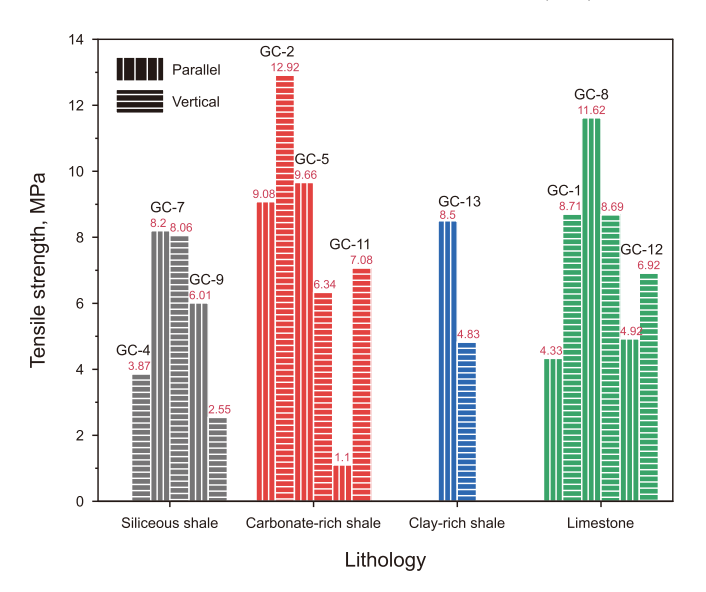


Fig. 12. Tensile strength of different lithologies.

could better reflect the brittleness of rock. The relationship between BI and other parameters (BI_M and different mineral content) was given in Fig. 14. It could be seen that there was an obvious positive correlation between BI_M and BI, that is, brittleness index was high when mineral brittleness was high. Therefore, the range of mechanical brittleness index could be inferred based on the mineral brittleness index after obtaining the rock mineral components. Specifically, the contribution of quartz mineral content to BI was positive, while that of carbonate mineral was negative. It could be considered that carbonate minerals were not brittle in the deep environment. As for the relationship between clay minerals content and BI, it was evident that two groups are gathering, which was related to lithology.

5.2. Reasons for high strength, high Young's modulus, and low brittleness of carbonate-rich shale

Carbonate-rich shale features high strength, high Young's modulus, and low brittleness compared to siliceous shale. There are two possible reasons for this feature:

- (1) The main minerals of this shale, quartz and carbonate, were presented at high contents of 40~50% and 30—40%, respectively. The quartz shows a high Young's modulus (96.5 GPa) and a low Poisson's ratio (0.06). The carbonate minerals contain mainly two types: calcite and dolomite, which exhibited high elastic modulus (74.4—124.4 GPa); resulting in the high strength and high Young's modulus of carbonaterich shale (Huo et al., 2018).
- (2) Unlike the low Poisson's ratio displayed by quartz, another characteristic of carbonate minerals was the high Poisson's ratio (0.32), mainly attributed to the special cleavage structure (three groups of the complete rhombic cleavage structure). As illustrated in Fig. 15, under triaxial compression, quartz minerals with the stable structure experiences brittle shear rupture; while carbonate minerals were prone to plastic shear slip along the cleavage structure, resulting in a high Poisson's ratio and thus plasticity enhancement.

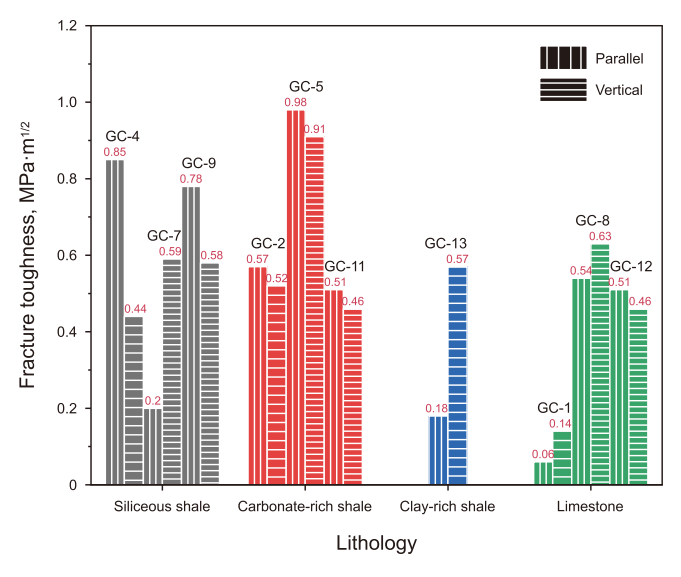


Fig. 13. Fracture toughness of different lithologies.

5.3. Morphology of hydraulic fractures in formation with difference between variable lithology

For reservoir stimulation, the morphology of hydraulic fractures could be different with varying lithologies. Siliceous shale with the relatively high quartz content was the preferred reservoir for fracturing. However, the high peak deviatoric stress and fracture toughness of siliceous shale increase the breakdown pressure and shorten the propagation distance in the reservoir (Fig. 16a). In carbonate-rich shale, the high content of both carbonate minerals and quartz enhanced the mechanical properties, further increasing the difficulty of hydraulic fracturing. Meanwhile, narrower primary hydraulic fractures and subtle secondary fractures would be detrimental to the proppant supporting and fracture conductivity (Fig. 16b). The increase of clay minerals contributed to the relatively lower mechanical parameters of the clay-rich shale, which would be beneficial for fracturing in this reservoir. With the decrease of mechanical parameters, fracturing energy could be saved after fracture initiation, which would promote the increase of hydraulic fractures propagation distance and activate bedding planes to create a complex fracture network (Fig. 16c). Compared with shale,

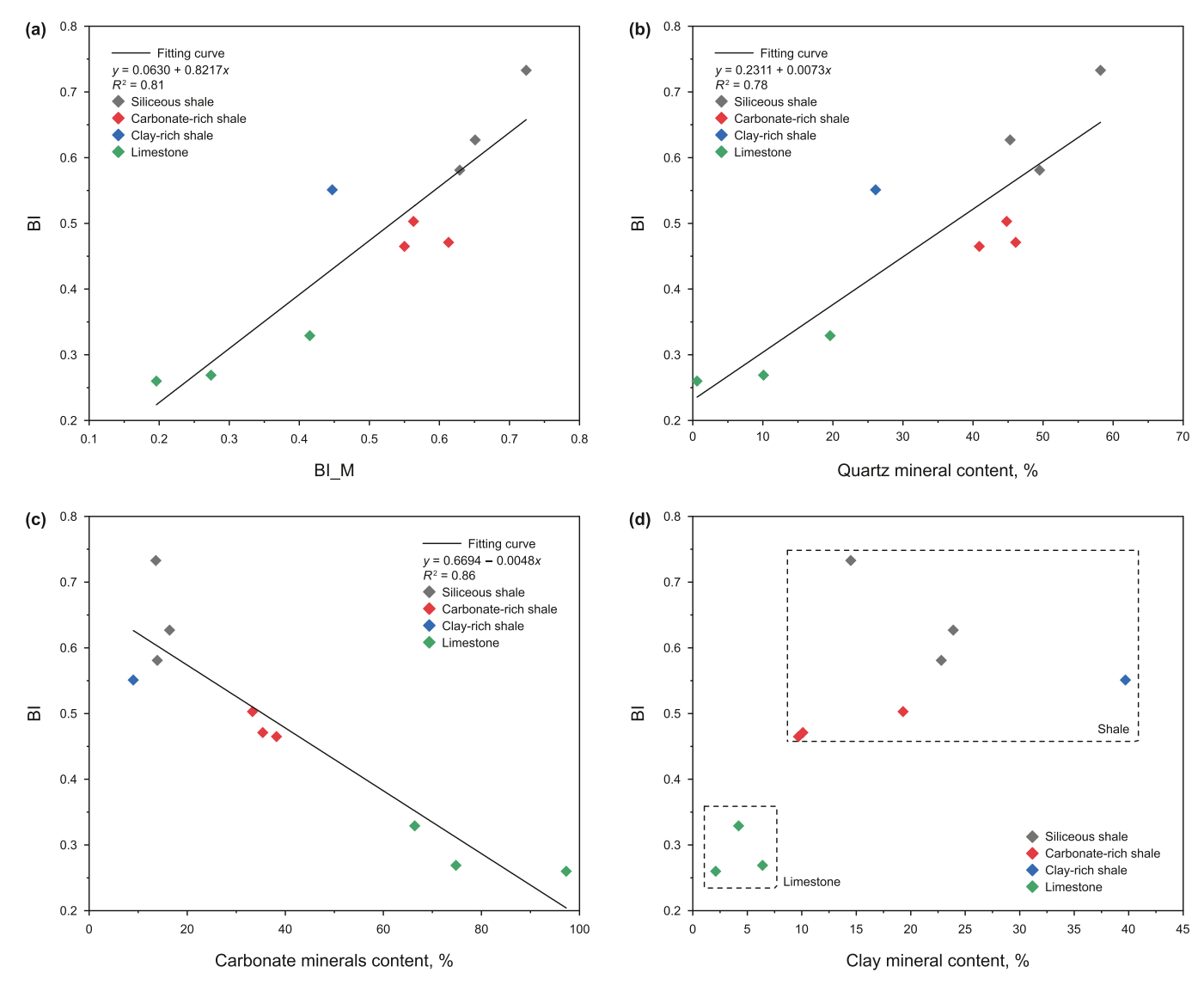


Fig. 14. Correlation analysis of BI with other parameters: (a) BI_M, (b) quartz, (c) carbonate minerals, and (d) clay.

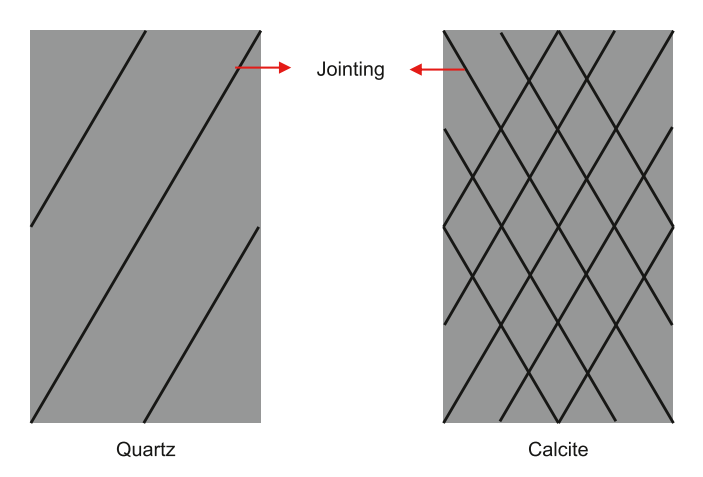


Fig. 15. Diagram of fracture in quartz and calcite under triaxial compression.

limestone would not only be unsuitable for fracturing but would also be an obstacle to the longitudinal extension of hydraulic fractures (Fig. 16d).

5.4. Recommended strategy for reservoir stimulation

The high *BI_M* and *BI* values in the W-2 member suggested that it was suitable for reservoir development given the previous analysis. However, the difficulty of developing different shales varies due to their different mechanical characteristics. For the development of the siliceous shale, the breakdown pressure was 96.5 MPa, the extension pressure was less than 65 MPa and the adding sand was convenient, according to the field data (Fig. 17a). Conversely, when carbonate-rich shale was developed, breakdown pressure and extensional pressure were 91.5 MPa and 88–90 MPa, respectively (Fig. 17b). Overall, treating pressure was at a high level. In addition, the difficulty in adding sand reflected the restricted fracture width, which was related to the characteristics of the carbonate-rich shale due to the increase in carbonate minerals.

For better stimulation of carbonate-rich shale reservoir, acid pretreatment measures could be considered. After acid treatment, carbonate minerals such as calcite are relatively reduced and quartz and clay minerals were relatively increased, which means that $BI_{-}M$ and $BI_{-}M$ values were also relatively increased. It would be conducive to increasing the inflow capacity with the complex microstructure and increased porosity (Chen et al., 2019b). Varying rock mechanical properties and fracture morphology will also favor the formation of complex networks (Tan et al., 2018). In summary, the measure for acid pretreatment should be considered.

5.5. Comparison between shales

Currently, the main commercially developed shale gas reservoirs were marine and continental shales. Due to different depositional environments, marine and continental shales were dominated by quartz (42-55.54%) and clay (13.1-67.2%) minerals, respectively (Tang et al., 2014; Yang et al., 2019; Chen et al., 2019a; Chen et al., 2022; He et al., 2022; Qiu et al., 2022). The carbonaterich shale, the main subject of this paper, was characterized by quartz (40.9-46.1%) and carbonate (33.3-38.2%) minerals. For quartz-dominated marine shales, quartz grains formed the rock skeleton, with clay minerals randomly distributed in the quartz skeleton, which was characterized by high compressive strength, high Young's modulus, and low Poisson's ratio. Continental shales with a clay skeleton exhibited lower compressive strength, lower Young's modulus, and higher Poisson's ratio. Carbonate-rich shales with quartz and calcite as rock skeleton featured higher compressive strength, higher Young's modulus, and higher Poisson's ratio. For example, the peak deviatoric stress, Young's modulus and Poisson's ratio of marine shale (under 80 MPa confining pressure) were 376.1 MPa, 26.90 GPa and 0.156, respectively, and those of continental shale (under 60 MPa confining pressure) were 128.6 MPa, 14.33 GPa and 0.175, respectively, while those of carbonate-rich shale (under 80 MPa confining pressure) were 630.66 MPa, 36.06 GPa and 0.199 (Wang et al., 2021b).

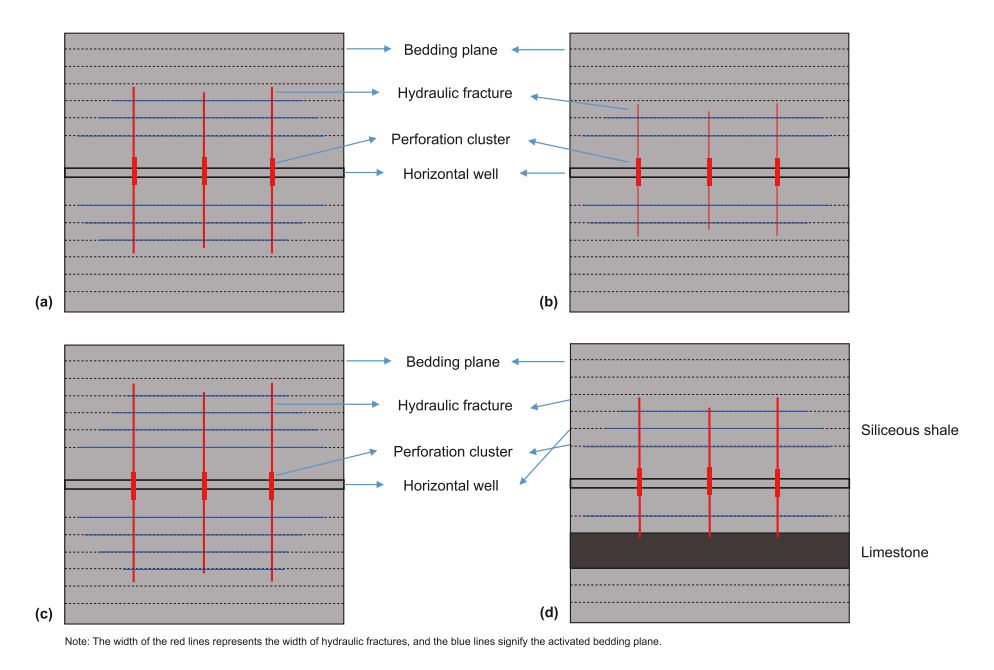


Fig. 16. Diagram of the contrast of morphology of hydraulic fractures in different lithology: (a) siliceous shale, (b) carbonate-rich shale, (c) clay-rich shale, and (d) siliceous shale with limestone interlayer.

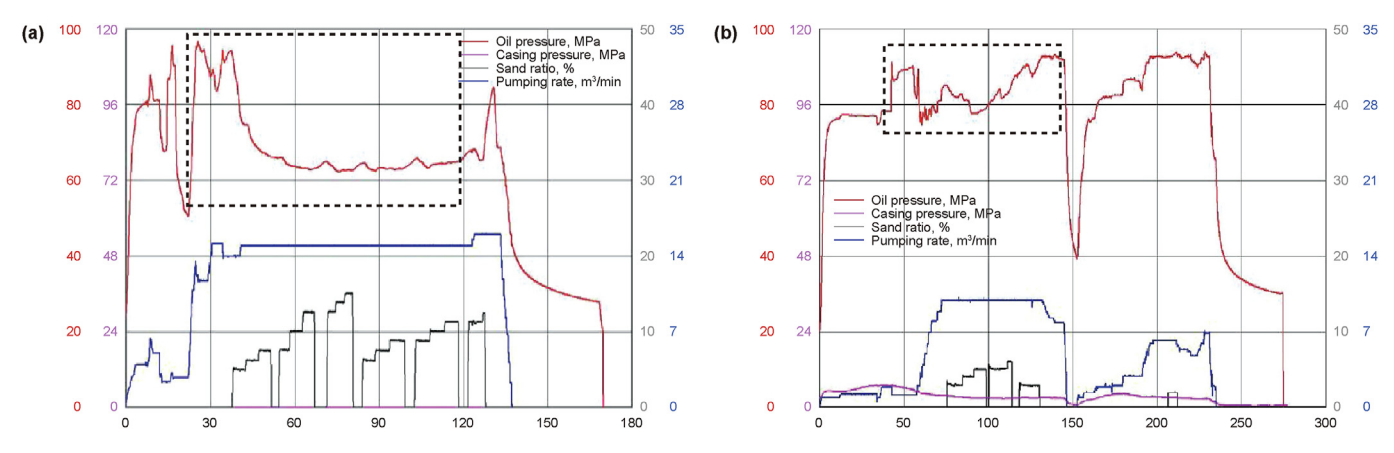


Fig. 17. Field pump pressure curves: (a) siliceous shale, and (b) carbonate-rich shale.

6. Conclusion

By performing systematic physical and mechanical tests of downhole cores from a new type of shale gas well, the mineral and mechanical properties of carbonate-rich shale were revealed. The conclusions are as follows:

- (1) Carbonate-rich shale possessed high compressive strength and high Young's modulus, which were improved by 10.74% and 3.37% compared to that of the siliceous shale. The carbonate-rich shale featured high tensile strength and fracture toughness, with insignificant anisotropy.
- (2) As the content of carbonate minerals increased (siliceous shale < carbonate-rich shale < limestone), the fracture morphology of specimens after triaxial compression transformed from brittle shear failure (sparse and wide fractures) to plastic shear slip (diffusely distributed and subtle fractures).
- (3) The brittleness index order was: siliceous shale, clay-rich shale, carbonate-rich shale, and limestone.
- (4) The special properties of carbonate-rich shale were rooted in the inherent feature of carbonate minerals (high strength, high elastic modulus, and cleavage structure) of carbonate minerals, resulting in greater challenge in reservoirs stimulation. Given this property, acid pretreatment should be considered for this type of reservoir.

CRediT authorship contribution statement

Zhen-Hui Bi: Data curation, Formal analysis, Writing — original draft. **Lei Wang:** Funding acquisition, Methodology, Writing — review & editing. **Chun-He Yang:** Project administration, Resources, Supervision. **Yin-Tong Guo:** Conceptualization, Methodology, Writing — review & editing. **Wu-Hao Guo:** Formal analysis, Methodology, Software. **Han-Zhi Yang:** Data curation, Investigation.

Declaration of competing interest

The authors declare that they have no known competing financial interests or personal relationships that could have appeared to influence the work reported in this paper.

Acknowledgements

This work was sponsored by the "National Natural Science

Foundation of China" (No. U22B6003), (No. 52104010), and (No. 52104046).

Appendix A. Supplementary data

Supplementary data to this article can be found online at https://doi.org/10.1016/j.petsci.2024.05.018.

References

Ai, C., Zhang, J., Li, Y., Zeng, J., Yang, X., Wang, J., 2016. Estimation criteria for rock brittleness based on energy analysis during the rupturing process. Rock Mech. Rock Eng. 49, 4681–4698. https://doi.org/10.1007/s00603-016-1078-x.

Altindag, R., 2002. The evaluation of rock brittleness concept on rotary blast hole drills. J. S. Afr. Inst. Min. Metall 102, 61–66. https://doi.org/10.1007/

Altowairqi, Y., Rezaee, R., Evans, B., Urosevic, M., 2015. Shale elastic property relationships as a function of total organic carbon content using synthetic samples. J. Petrol. Sci. Eng. 133, 392–400. https://doi.org/10.1016/j.petrol.2015.06.028.

Atkinson, C., Smelser, R.E., Sanchez, J., 1982. Combined mode fracture via the cracked Brazilian disk test. Int. J. Fract. 18, 279–291. https://doi.org/10.1007/BF00015688.

Chang, X., Xu, E.S., Guo, Y.T., Yang, C.H., Hu, Z.W., Guo, W.H., 2022. Experimental study of hydraulic fracture initiation and propagation in deep shale with different injection methods. J. Petrol. Sci. Eng. 216, 110834. https://doi.org/ 10.1016/j.petrol.2022.110834.

Chen, K.F., Liu, X.P., Liu, J., Zhang, C., Guan, M., Zhou, S.X., 2019. Lithofacies and pore characterization of continental shale in the second member of the kongdian formation in the cangdong sag, bohai bay basin, China. J. Petrol. Sci. Eng. 177, 154–166. https://doi.org/10.1016/j.petrol.2019.02.022.

Chen, T.Y., Lai, G.M., Cheng, Z.Y., Sun, Q., Liu, S., 2019. Experimental study on pore evolution of Longmaxi shale under acidification. Meitan Xuebao/J.China Coal Soc. 44, 3480–3490. https://doi.org/10.13225/j.cnki.jccs.2018.1511 (in Chinese).

Chen, X.L., Shi, W.Z., Hu, Q.H., Hou, Y.G., Zhai, G.Y., Dong, T., Zhou, Z., Du, X.B., 2022. Origin of authigenic quartz in organic-rich shales of the Niutitang Formation in the northern margin of Sichuan Basin, South China: implications for pore network development. Mar. Petrol. Geol. 138, 105548. https://doi.org/10.1016/ j.marpetgeo.2022.105548.

Fan, Z.D., Ren, L., Xie, H.P., Zhang, R., Li, C.B., Lu, H., Zhang, A.L., Zhou, Q., Ling, W.Q., 2022. 3D anisotropy in shear failure of a typical shale. Petrol. Sci. https:// doi.org/10.1016/j.petsci.2022.10.017.

Gao, H.K., Wang, Q., Jiang, B., Zhang, P., Jiang, Z.H., Wang, Y., 2021. Relationship between rock uniaxial compressive strength and digital core drilling parameters and its forecast method. Int J Coal Sci Technol 8, 605–613. https://doi.org/ 10.1007/s40789-020-00383-4.

Gholami, R., Rasouli, V., Sarmadivaleh, M., Minaeian, V., Fakhari, N., 2016. Brittleness of gas shale reservoirs: a case study from the north Perth basin, Australia. J. Nat. Gas Sci. Eng. 33, 1244–1259. https://doi.org/10.1016/j.jngse.2016.03.013.

Guo, T.L., Zhang, H.R., 2014. Formation and enrichment mode of Jiaoshiba shale gas field, Sichuan Basin. Petrol. Explor. Dev. 41, 31–40. https://doi.org/10.1016/

Guo, X.S., Hu, D.F., Li, Y.P., Wei, Z.H., Liu, Z.J., 2017. Geological factors controlling shale gas enrichment and high production in Fuling shale gas field. Petrol. Explor. Dev. 44, 481–491. https://doi.org/10.11698/PED.2017.04.01.

Guo, W.H., Guo, Y.T., Yang, C.H., Wang, L., Chang, X., Yang, H.Z., Bi, Z.H., 2022a. Experimental investigation on the effects of heating-cooling cycles on the physical and mechanical properties of shale. J. Nat. Gas Sci. Eng. 97, 104377.

https://doi.org/10.1016/j.jngse.2021.104377.

- Guo, W.H., Guo, Y.T., Yang, H.Z., Wang, L., Liu, B.H., Yang, C.H., 2022b. Tensile mechanical properties and AE characteristics of shale in triaxial Brazilian splitting tests. J. Petrol. Sci. Eng. 219, 111080. https://doi.org/10.1016/j.petrol.2022.111080.
- Hajiabdolmajid, V., Kaiser, P., 2003. Brittleness of rock and stability assessment in hard rock tunneling. Tunn. Undergr. Space Technol. 18, 35–48. https://doi.org/10.1016/S0886-7798(02)00100-1.
- Hassan, N.F., Jimoh, O.A., Shehu, S.A., Hareyani, Z., 2019. The effect of mineralogical composition on strength and drillability of granitic rocks in hulu langat, selangor Malaysia. Geotech. Geol. Eng. 37, 5499–5505. https://doi.org/10.1007/ s10706-019-00995-x.
- Hatheway, A.W., 2009. The complete ISRM suggested methods for rock characterization, testing and monitoring; 1974-2006. Environ. Eng. Geosci. 15, 47–48. https://doi.org/10.2113/gseegeosci.15.1.47.
- He, W.H., Chen, K.Y., Hayatdavoudi, A., Sawant, K., Lomas, M., 2019. Effects of clay content, cement and mineral composition characteristics on sandstone rock strength and deformability behaviors. J. Petrol. Sci. Eng. 176, 962–969. https:// doi.org/10.1016/j.petrol.2019.02.016.
- He, Q.Y., Li, D.L., Sun, Q., Wei, B.W., Wang, S.F., 2022. Main controlling factors of marine shale compressive strength: a case study on the cambrian Niutitang Formation in Dabashan Mountain. Energy 260, 125100. https://doi.org/10.1016/ i.energy.2022.125100.
- Heng, S., Guo, Y.T., Yang, C.H., Daemen, J.J.K., Li, Z., 2015. Experimental and theoretical study of the anisotropic properties of shale. Int. J. Rock Mech. Min. Sci. 74, 58–68. https://doi.org/10.1016/j.ijrmms.2015.01.003.
- Heng, S., Li, X.Z., Liu, X., Chen, Y., 2020. Experimental study on the mechanical properties of bedding planes in shale. J. Nat. Gas Sci. Eng. 76, 103161. https://doi.org/10.1016/j.jngse.2020.103161.
- Hou, B., Zhang, R.X., Zeng, Y.J., Fu, W.N., Muhadasi, Y., Chen, M., 2018. Analysis of hydraulic fracture initiation and propagation in deep shale formation with high horizontal stress difference. J. Petrol. Sci. Eng. 170, 231–243. https://doi.org/ 10.1016/j.petrol.2018.06.060.
- Hucka, V., Das, B., 1974. Brittleness determination of rocks by different methods. Int. J. Rock Mech. Min. Sci. Geomech. Abstracts 11, 389–392. https://doi.org/ 10.1016/0148-9062(74)91109-7.
- Huo, Z.P., Zhang, J.C., Li, P., Tang, X., Yang, X., Qiu, Q.L., Dong, Z., Li, Z., 2018. An improved evaluation method for the brittleness index of shale and its application a case study from the southern north China basin. J. Nat. Gas Sci. Eng. 59, 47–55. https://doi.org/10.1016/j.jngse.2018.08.014.
- Jarvie, D.M., Hill, R.J., Ruble, T.E., Pollastro, R.M., 2007. Unconventional shale-gas systems: the Mississippian Barnett Shale of north-central Texas as one model for thermogenic shale-gas assessment. Bulletin 91, 475–499. https://doi.org/ 10.1306/12190606068.
- Jin, X.C., Shah, S.N., Roegiers, J.C., Zhang, B., 2015. An integrated petrophysics and Geomechanics approach for fracability evaluation in shale reservoirs. SPE J. 20, 518–526. https://doi.org/10.2118/168589-PA.
- Kurtulus, C., Caklr, S., Yoğurtcuoğlu, A.C., 2016. Ultrasound study of limestone rock physical and mechanical properties. Soil Mech. Found. Eng. 52, 348–354. https://doi.org/10.1007/s11204-016-9352-1.
- Labani, M.M., Rezaee, R., 2015. The importance of geochemical parameters and shale composition on rock mechanical properties of gas shale reservoirs: a case study from the kockatea shale and carynginia formation from the perth basin, western Australia. Rock Mech. Rock Eng. 48, 1249–1257. https://doi.org/10.1007/s00603-014-0617-6.
- Lai, J., Wang, G.W., Huang, L.X., Li, W.L., Ran, Y., Wang, D., Zhou, Z.L., Chen, J., 2015. Brittleness index estimation in a tight shaly sandstone reservoir using well logs. J. Nat. Gas Sci. Eng. 27, 1536–1545. https://doi.org/10.1016/j.jngse.2015.10.020.
- Lei, B., Zuo, J.P., Liu, H.Y., Wang, J.T., Xu, F., Li, H.T., 2021. Experimental and numerical investigation on shale fracture behavior with different bedding properties. Eng. Fract. Mech. 247, 107639. https://doi.org/10.1016/j.engfracmech.2021.107639.
- Li, Q.H., Chen, M., Jin, Y., Hou, B., Zhang, B.W., 2012. Indoor evaluation method for shale brittleness and improvement. Yanshilixue Yu Gongcheng Xuebao/Chinese J.Rock Mecha.Engineer. 31, 1680–1685.
- Li, N., Zou, Y.S., Zhang, S.C., Ma, X.F., Zhu, X.W., Li, S.H., Cao, T., 2019. Rock brittleness evaluation based on energy dissipation under triaxial compression. J. Petrol. Sci. Eng. 183, 106349. https://doi.org/10.1016/j.petrol.2019.106349.
- Li, Y.J., Song, L.H., Tang, Y.J., Zuo, J.P., Xue, D.J., 2022. Evaluating the mechanical properties of anisotropic shale containing bedding and natural fractures with discrete element modeling. Int J Coal Sci Technol 9, 18. https://doi.org/10.1007/s40789-022-00473-5.
- Liang, X.W., Li, L., 2021. Geological conditions and exploration potential for shale gas in Upper Permian Wujiaping Formation in the region of western Hubei-eastern Chongqing. Petrol.Geo.Exper. 43, 386–394. https://doi.org/10.11781/ svsvdz202103386.
- Liang, Q.S., Zhang, X., Tian, J.C., Sun, X., Chang, H.L., 2018. Geological and geochemical characteristics of marine-continental transitional shale from the lower permian taiyuan formation, taikang uplift, southern north China basin. Mar. Petrol. Geol. 98, 229—242. https://doi.org/10.1016/ j.marpetgeo.2018.08.027.
- Liu, J.S., Ding, W.L., Wang, R.Y., Wu, Z.H., Gong, D.J., Wang, X.H., Yin, S., Jiao, B.C., 2018. Quartz types in shale and their effect on geomechanical properties: an example from the lower Cambrian Niutitang Formation in the Cen'gong block, South China. Appl. Clay Sci. 163, 100–107. https://doi.org/10.1016/j.clay.2018.07.019.
- Lu, H.J., Xie, H.P., Luo, Y., Ren, L., Zhang, R., Li, C.B., Wang, J., Yang, M.Q., 2021. Failure

- characterization of Longmaxi shale under direct shear mode loadings. Int. J. Rock Mech. Min. Sci. 148, 104936. https://doi.org/10.1016/j.ijrmms.2021.104936.
- Ma, T.S., Wang, H.N., Liu, Y., Fu, C.L., Ranjith, P.G., 2023. Experimental investigation on the anisotropy of mode-I fracture and tensile failure of layered shale. Eng. Fract. Mech. 290, 109484. https://doi.org/10.1016/j.engfracmech.2023.109484.
- Mahanta, B., Singh, T.N., Ranjith, P.G., Vishal, V., 2018. Experimental investigation of the influence of strain rate on strength; failure attributes and mechanism of Jhiri shale. J. Nat. Gas Sci. Eng. 58, 178–188. https://doi.org/10.1016/ i.ingse.2018.08.001.
- Martin, C.D., 1996. Brittle failure of rock materials: test results and constitutive models. Can. Geotech. J. 33, 378. https://doi.org/10.1139/t96-901, 378.
- Mo, Y.C., Zuo, S.Y., Wang, L., 2022. Mechanical characteristics of thick-bedded limestone with different bedding angles subjected to acid corrosion. Bull. Eng. Geol. Environ. 81, 166. https://doi.org/10.1007/s10064-022-02667-2.
- Munoz, H., Taheri, A., Chanda, E.K., 2016. Fracture energy-based brittleness index development and brittleness quantification by pre-peak strength parameters in rock uniaxial compression. Rock Mech. Rock Eng. 49, 4587–4606. https:// doi.org/10.1007/s00603-016-1071-4.
- Qiu, Z., Liu, B., Lu, B., Shi, Z.S., Li, Z.Y., 2022. Mineralogical and petrographic characteristics of the Ordovician-Silurian Wufeng-Longmaxi Shale in the Sichuan Basin and implications for depositional conditions and diagenesis of black shales. Mar. Petrol. Geol. 135, 105428. https://doi.org/10.1016/j.marpetgeo.2021.105428.
- Rahimzadeh Kivi, I., Zare-Reisabadi, M., Saemi, M., Zamani, Z., 2017. An intelligent approach to brittleness index estimation in gas shale reservoirs: a case study from a western Iranian basin. J. Nat. Gas Sci. Eng. 44, 177–190. https://doi.org/ 10.1016/j.ingse.2017.04.016.
- Rahimzadeh Kivi, I., Ameri, M., Molladavoodi, H., 2018. Shale brittleness evaluation based on energy balance analysis of stress-strain curves. J. Petrol. Sci. Eng. 167, 1–19. https://doi.org/10.1016/j.petrol.2018.03.061.
- Rickman, R., Mullen, M., Petre, E., Grieser, B., Kundert, D., 2008. A practical use of shale petrophysics for stimulation design optimization: all shale plays are not clones of the barnett shale. Presented at the SPE Annual Technical Conference and Exhibition, OnePetro. https://doi.org/10.2118/115258-MS.
- Rybacki, E., Reinicke, A., Meier, T., Makasi, M., Dresen, G., 2015. What controls the mechanical properties of shale rocks? Part I: strength and Young's modulus. J. Petrol. Sci. Eng. 135, 702—722. https://doi.org/10.1016/j.petrol.2015.10.028.
- Rybacki, E., Meier, T., Dresen, G., 2016. What controls the mechanical properties of shale rocks? – Part II: brittleness. J. Petrol. Sci. Eng. 144, 39–58. https://doi.org/ 10.1016/j.petrol.2016.02.022.
- Shi, X.S., Yao, W., Liu, D.A., Xia, K.W., Tang, T.W., Shi, Y.R., 2019. Experimental study of the dynamic fracture toughness of anisotropic black shale using notched semi-circular bend specimens. Eng. Fract. Mech. 205, 136–151. https://doi.org/ 10.1016/j.engfracmech.2018.11.027.
- Sone, H., Zoback, M.D., 2013. Mechanical properties of shale-gas reservoir rocks Part 1: static and dynamic elastic properties and anisotropy. Geophy. 78, D381–D392. https://doi.org/10.1190/geo2013-0050.1.
- Song, X.H., Guo, Y.T., Zhang, J., Sun, N.N., Shen, G.F., Chang, X., Yu, W.S., Tang, Z.Y., Chen, W., Wei, W., Wang, L., Zhou, J., Li, X., Li, X.F., Zhou, J.H., Xue, Z., 2019. Fracturing with carbon dioxide: from microscopic mechanism to reservoir application. Joule 3, 1913—1926. https://doi.org/10.1016/j.joule.2019.05.004.
- Tan, P., Jin, Y., Han, K., Hou, B., Chen, M., Guo, X.F., Gao, J., 2017. Analysis of hydraulic fracture initiation and vertical propagation behavior in laminated shale formation. Fuel 206, 482–493. https://doi.org/10.1016/j.fuel.2017.05.033.
- Tan, P., Jin, Y., Han, L., Shan, Q.L., Zhang, Y.K., Chen, G., Zhou, Y.C., 2018. Influencing mechanism of acidification pretreatment on hydraulic fracture for deep fractured shale reservoirs. Yantu Gongcheng Xuebao/Chin. J. Geotech. Eng. 40, 384–390. https://doi.org/10.11779/CJGE201802021.
- Tang, X., Zhang, J.C., Wang, X.Z., Yu, B.S., Ding, W.L., Xiong, J.Y., Yang, Y.T., Wang, L., Yang, C., 2014. Shale characteristics in the southeastern Ordos Basin, China: implications for hydrocarbon accumulation conditions and the potential of continental shales. Int. J. Coal Geol. 128–129, 32–46. https://doi.org/10.1016/j.coal.2014.03.005.
- Tarasov, B., Potvin, Y., 2013. Universal criteria for rock brittleness estimation under triaxial compression. Int. J. Rock Mech. Min. Sci. 59, 57–69. https://doi.org/ 10.1016/j.ijrmms.2012.12.011.
- Wang, R.Y., Ding, W.L., Zhang, Y.Q., Wang, Z., Wang, X.H., He, J.H., Zeng, W.T., Dai, P., 2016. Analysis of developmental characteristics and dominant factors of fractures in Lower Cambrian marine shale reservoirs: a case study of Niutitang formation in Cen'gong block, southern China. J. Petrol. Sci. Eng. 138, 31–49. https://doi.org/10.1016/j.petrol.2015.12.004.
- Wang, L., Guo, Y.T., Yang, C.H., Xiao, J.L., Lu, C.S., Song, Y.F., 2020. Mechanical characterization of continental shale in Sichuan Basin of China and its potential impact on reservoir stimulation. J. Nat. Gas Sci. Eng. 79, 103346. https://doi.org/10.1016/j.jngse.2020.103346.
- Wang, L., Guo, Y.T., Zhou, J., Yang, H.Z., Yang, C.H., Xiao, J.L., 2021a. Rock mechanical characteristics of deep marine shale in southern China, a case study in Dingshan block. J. Petrol. Sci. Eng. 204, 108699. https://doi.org/10.1016/ j.petrol.2021.108699.
- Wang, L., Yang, H.Z., Guo, Y.T., Bi, Z.H., Guo, W.H., Yang, C.H., 2021b. Comparative study of marine and lacustrine shale reservoirs from the viewpoint of rock mechanics. Energy Fuels 35, 19481–19495. https://doi.org/10.1021/ acs.energyfuels.1c03312.
- Wang, P.W., Liu, Z.B., Li, X., Liu, H.T., Zhou, L., Xiao, X., Wang, R.Y., 2022. Development of the Upper Permian Wujiaping shale in Hongxing area, eastern Sichuan

- Basin, and its significance to shale gas enrichment. Oil Gas Geol. 43, 1102. https://doi.org/10.11743/ogg20220508.
- Wang, H.N., Ma, T.S., Liu, Y., Wu, B.S., Ranjith, P.G., 2023. Numerical and experimental investigation of the anisotropic tensile behavior of layered rocks in 3D space under Brazilian test conditions. Int. J. Rock Mech. Min. Sci. 170, 105558. https://doi.org/10.1016/j.ijrmms.2023.105558.
- Wen, T., Tang, H.M., Wang, Y.K., 2020. Brittleness evaluation based on the energy evolution throughout the failure process of rocks. J. Petrol. Sci. Eng. 194, 107361. https://doi.org/10.1016/j.petrol.2020.107361.
- Wu, J., Liang, C., Yang, R.C., Hu, Z., Li, W., Xie, J., 2022. The genetic relationship between paleoenvironment, mineral compositions and lithofacies in the Ordovician—Silurian Wufeng—Longmaxi sedimentary succession in the Sichuan Basin, SW China. J. Asian Earth Sci. 236, 105334. https://doi.org/10.1016/ i.iseaes.2022.105334.
- Xie, J., 2018. Rapid shale gas development accelerated by the progress in key technologies: a case study of the Changning-Weiyuan National Shale Gas Demonstration Zone. Nat. Gas. Ind. B 5, 283–292. https://doi.org/10.1016/ i.ngib.2017.12.007.
- Xiong, J., Liu, K.Y., Shi, C.Y., Liu, X.J., Huang, L.L., 2021. Logging prediction and evaluation of fracture toughness for the shales in the Longmaxi Formation, southern sichuan basin. Petroleum 7, 254–262. https://doi.org/10.1016/ i.petlm.2020.10.003.
- Xu, W.J., Zhao, Y.X., Wang, L., Jiang, F., 2022. Experimental investigation of hydraulic fracture propagation behavior in layered continental shale. Energy Rep. 8, 14362–14373. https://doi.org/10.1016/j.egyr.2022.10.429.
 Xue, C.Q., Wu, J.G., Qiu, L.W., Zhong, J.H., Zhang, S.R., Zhang, B., Wu, X., Hao, B., 2020.
- Xue, C.Q., Wu, J.G., Qiu, L.W., Zhong, J.H., Zhang, S.R., Zhang, B., Wu, X., Hao, B., 2020. Lithofacies classification and its controls on the pore structure distribution in Permian transitional shale in the northeastern Ordos Basin, China. J. Petrol. Sci. Eng. 195, 107657. https://doi.org/10.1016/j.petrol.2020.107657.
- Yang, R., Hu, Q.H., Yi, J.Z., Zhang, B.Q., He, S., Guo, X.W., Hou, Y.G., Dong, T., 2019. The effects of mineral composition, TOC content and pore structure on spontaneous imbibition in Lower Jurassic Dongyuemiao shale reservoirs. Mar. Petrol. Geol. 109, 268–278. https://doi.org/10.1016/j.marpetgeo.2019.06.003.
- 109, 268–278. https://doi.org/10.1016/j.marpetgeo.2019.06.003.

 Yu, K., Shao, C.J., Ju, Y.W., Qu, Z.H., 2019. The genesis and controlling factors of micropore volume in transitional coal-bearing shale reservoirs under different

- sedimentary environments. Mar. Petrol. Geol. 102, 426–438. https://doi.org/10.1016/j.marpetgeo.2019.01.003.
- Zhang, D., 2021. Development prospect of natural gas industry in the Sichuan Basin in the next decade. Nat. Gas. Ind. 41, 34–45. https://doi.org/10.3787/j.issn.1000-0976 2021 08 004
- Zhang, W.Q., Lv, C., 2020. Effects of mineral content on limestone properties with exposure to different temperatures. J. Petrol. Sci. Eng. 188, 106941. https://doi.org/10.1016/j.petrol.2020.106941.
- Zhang, D., Ranjith, P.G., Perera, M.S.A., 2016. The brittleness indices used in rock mechanics and their application in shale hydraulic fracturing: a review. J. Petrol. Sci. Eng. 143, 158–170. https://doi.org/10.1016/i.petrol.2016.02.011.
- Zhang, B., Wen, H.G., Qing, H.R., Yang, K., Luo, Y., Yang, H.Y., Wang, P.W., He, L.F., Xiao, W., 2022. The influence of depositional and diagenetic processes on rock electrical properties: a case study of the Longmaxi shale in the Sichuan Basin. J. Petrol. Sci. Eng. 211, 110119. https://doi.org/10.1016/j.petrol.2022.110119.
- Zhao, Z., Li, X., He, J., Mao, T., Li, C., Zheng, B., 2018a. Investigation of fracture propagation characteristics caused by hydraulic fracturing in naturally fractured continental shale. J. Nat. Gas Sci. Eng. 53, 276–283. https://doi.org/10.1016/ i.ingse.2018.02.022.
- Zhao, Z.H., Li, X., He, J.M., Mao, T.Q., Li, G.F., Zheng, B., 2018b. A laboratory investigation of fracture propagation induced by supercritical carbon dioxide fracturing in continental shale with interbeds. J. Petrol. Sci. Eng. 166, 739–746. https://doi.org/10.1016/j.petrol.2018.03.066.
- Zhao, J.Z., Ren, L., Jiang, T.X., Hu, D.F., Wu, L.Z., Wu, J.F., Yin, C.B., Li, Y.M., Hu, Y.Q., Lin, R., Li, X.G., Peng, Y., Shen, C., Chen, X.Y., Yin, Q., Jia, C.G., Song, Y., Wang, H.T., Li, Z.Y., Wu, J.J., Zeng, B., Du, L.L., 2022. Ten years of gas shale fracturing in China: review and prospect. Nat. Gas. Ind. B 9, 158–175. https://doi.org/10.1016/j.ngib.2022.03.002.
- Zou, C.N., Dong, D.Z., Wang, S.J., Li, J.Z., Li, X.J., Wang, Y.M., Li, D.H., Cheng, K.M., 2010. Geological characteristics and resource potential of shale gas in China. Petrol. Explor. Dev. 37, 641–653. https://doi.org/10.1016/S1876-3804(11)60001-3
- Zou, C.N., Zhao, Q., Cong, L.Z., Wang, H.Y., Shi, Z.S., Wu, J., Pan, S.Q., 2021. Development progress, potential and prospect of shale gas in China. Nat. Gas. Ind. 41, 1–14. https://doi.org/10.3787/j.issn.1000-0976.2021.01.001.